



“BABES-BOLYAI” UNIVERSITY
FACULTY OF PHYSICS

Dana Găvre

*The study of the vitreous matrix composition influence on
transitional ions behavior*

Ph.D Thesis Summary

Scientific supervisor
Prof. Univ. Dr. Ioan Ardelean

Cluj-Napoca
2010

Table of contents

Introduction	6
Chapter 1. Oxide materials with vitreous structure	9
1.1. Introductory idea	9
1.1.1. Non crystalline solid, crystalline, amorphous and vitreous structures	9
1.1.2. Vitreous transition	10
1.2. Oxide materials with vitreous structure synthesis	12
1.2.1. Materials for glasses industry	12
1.2.2. Oxide materials with vitreous structure synthesis	15
1.2.3. Oxide materials with vitreous structure synthesis using undercooling melted method	16
1.2.4. Oxide materials with vitreous structure synthesis using other methods	17
1.3. Crystalline and vitreous structure of P ₂ O ₅	19
1.4. Oxide glasses application	24
1.4.1. Semiconductor oxide glasses	24
1.4.2. Controllable corrosion glasses in biological	25
1.4.3. Radiotherapeutic glasses	26
1.4.4. Bioactive oxide glasses	26
1.4.5. Oxide glasses with properties for storage of radioactive waste	27
1.4.6. Other applications of oxide glasses	27
References	28
Chapter 2. Some study methods of vitreous oxide materials structure	31
2.1. X-Ray Diffraction	31
2.1.1. Noncrystalline phases identification	32
2.2. Infrared absorption spectroscopy	34
2.2.1. Vibration types	37
2.3. Raman Spectroscopy	38
2.3.1. Structural information obtained from Raman measurements	41
2.3.2. Raman and IR spectroscopy complementarities	42
2.4. Electron Paramagnetic Resonance	43
2.4.1. EPR spectra characteristics of Mn ²⁺ ions	47

References	49
Chapter 3. Experimental techniques	50
3.1. The processing and preparation of the samples	50
3.2. Experimental techniques used for samples measurements	52
3.2.1. X-Ray diffraction spectra	52
3.2.2. IR absorption spectra	54
3.2.3. Raman spectra	55
3.2.4. RPE spectra	59
References	61
Chapter 4. The results of $x\text{MnO} \cdot (100-x)[y\text{P}_2\text{O}_5 \cdot \text{CaO}]$ phosphate glasses study	62
4.1. Structural characteristics of $[y\text{P}_2\text{O}_5 \cdot \text{CaO}]$ binary glasses	62
4.1.1. Comparative study by X-Ray diffraction of $[y\text{P}_2\text{O}_5 \cdot \text{CaO}]$ glasses structure	62
4.1.2. Comparative study by IR absorption of $[y\text{P}_2\text{O}_5 \cdot \text{CaO}]$ glasses structure	64
4.1.3. Comparative study by Raman effect of $[y\text{P}_2\text{O}_5 \cdot \text{CaO}]$ glasses structure	70
Conclusions	73
References	74
4.2. Structural characteristics of $x\text{MnO} \cdot (100-x)[y\text{P}_2\text{O}_5 \cdot \text{CaO}]$ ternary glasses	76
4.2.1. Comparative study by IR absorption of $x\text{MnO} \cdot (100-x)[y\text{P}_2\text{O}_5 \cdot \text{CaO}]$ glasses structure	76
4.2.2. Comparative study by Raman effect of $x\text{MnO} \cdot (100-x)[y\text{P}_2\text{O}_5 \cdot \text{CaO}]$ glasses structure	91
4.2.3. Comparative study by EPR of $x\text{MnO} \cdot (100-x)[y\text{P}_2\text{O}_5 \cdot \text{CaO}]$ glasses structure	96
Conclusions	110
References	115

Introduction

Phosphate glasses are both scientifically and technologically important materials because they generally offer some unique physical properties better than other glasses, such as high thermal expansion coefficients, low melting and softening temperatures, ultraviolet (UV) transmission and optical characteristics. However, their poor chemical durability limits their use in many applications. One approach in order to increase the chemical durability is to add various oxides to phosphate glasses. Specific properties of phosphate glasses can be understood only if their behavior over the entire composition range is known, which is also of interest with regard to changes of certain macroscopic properties.

The study presented in this thesis has as objective the obtaining of new experimental data and the clarification of the physical phenomenon that determines the structural behavior of P_2O_5 based glasses with CaO like network modification and doped with manganese ions. In order to obtain these information $xMnO \cdot (100-x)[yP_2O_5 \cdot CaO]$ glass systems, where $0 \leq x \leq 50$ mol % and $y = 3 \div 1$, were prepared and investigated by X-ray diffraction, IR spectroscopy, Raman spectroscopy and electron paramagnetic resonance.

The thesis is structured in four chapters. In the first chapter are presented general concept regarding vitreous oxide materials, the crystalline and vitreous structure of P_2O_5 and the applications of phosphate glasses. The second chapter presents theoretical aspects about the study methods used in determination of the structural properties of the investigated glasses. In the third chapter are presented information regarding the preparation mode and also the experimental techniques used. In forth chapter are presented and discussed the experimental results obtained for the investigated glasses. In the end are presented the general conclusions which evidenced the most important results of this thesis.

Keywords: phosphate glasses, X-ray diffraction, IR spectroscopy, Raman spectroscopy, EPR, manganese ions.

Chapter 1

Oxide materials with vitreous structure

The glass former component in phosphate glasses is P_2O_5 . The basic building blocks of crystalline and amorphous phosphates are the PO_4 tetrahedra, which link via covalent bridging oxygens to form various phosphate anions. These tetrahedra units can be classified using Q-site model [20]. Based on this model, the phosphate anions can be described using Q^i terminology, where “i” represents the number of bridging oxygens per tetrahedron. These tetrahedra are: Q^3 – cross-linked three dimensional network, Q^2 – metaphosphate chains and rings, Q^1 – pyrophosphate groups and Q^0 – orthophosphate groups.

P_2O_5 is different from the other single component glass-former due to the existence of a terminal oxygen on each network forming cation. This terminal oxygen is a short double – bonded (P=O) bond, with a significant π -bond character that accounts for the additional valence electron. The presence of such terminating oxygens results in less cross-linked phosphate glass structure compared to silicate glasses.

Chapter 2

Some study methods of vitreous oxide materials structure

This chapter presents some of the methods used in the investigation of the structure and properties of vitreous systems. In this study X-ray diffraction, IR and Raman spectroscopies and electron paramagnetic resonance were chosen as investigation methods.

X-ray diffraction offers useful information regarding the structure of the crystalline solid, information which can be used to determine the simple and complex molecular structures. In addition, the x-ray diffraction is the most used method to determine the vitreous or crystalline state of a material.

IR absorption spectroscopy is used to obtain information connected to the structure of the compound. The radiation is absorbed by organic molecules and converted in molecular vibration energy. When the radiant energy coincides with a specific molecular vibration, the absorption appears. The wavenumbers at which the

radiation is absorbed by the organic molecule gives information regarding the functional groups presented in the molecule.

The Raman spectroscopy, complementary to IR spectroscopy, brings useful contributions to the molecular vibrations study. The interaction mechanism of electromagnetic radiation with the molecular vibration, which sits at Raman spectroscopy basis, differs from the one of the process that sits at IR spectroscopy basis. The Raman effect is induced by the variation of electronic charge distribution under the effect of the electromagnetic applied radiation and not by the variation of nuclear charge distribution from the molecule.

RPE is a method widely used to describe the fundamental states and to characterize the vicinities effect on the energetic levels of the paramagnetic centers. The methods consist in the study of the electronics levels split of the atoms in the presence of a external magnetic field. This method is one of the most powerful techniques for local order investigation.

Chapter 3

Experimental techniques

The $x\text{MnO} \cdot (100-x)[y\text{P}_2\text{O}_5 \cdot \text{CaO}]$ glass system, with $y = 1 \div 3$ and $0 \leq x \leq 50$ mol % MnO, were prepared using reagent grade compounds, i.e. MnCO_3 , $(\text{NH}_4)_2\text{HPO}_4$ and CaCO_3 in suitable proportions. The mixtures corresponding to the desired compositions were mechanically homogenized, placed in sintered corundum crucibles and melted in air in an electric furnace at 1200°C . The molten material was kept at this temperature for 5 minutes and then quenched at room temperature by pouring on the stainless-steel plates.

The structure of the samples were analyzed by X-ray diffraction, using powders, with a D8 Advance Bruker diffractometer.

Infrared spectra were obtained in the $400\text{-}4000\text{ cm}^{-1}$ spectral range and it was analyzed especially in the $400\text{-}1600\text{ cm}^{-1}$ regions with a JASCO 6100 FT-IR spectrometer by using the KBr pellet technique. The spectral resolution used for the recording of the IR spectra was 2 cm^{-1} . In order to obtain good quality spectra, the samples were crushed in an agate mortar to obtain particles of micrometer size. This

procedure was applied every time to fragments of bulk glass to avoid structural modifications due to ambient moisture.

The Raman spectra were collected at room temperature using a JASCO NRS-3300 micro-Raman Spectrometer with an air cooled CCD detector in a backscattering geometry and using a 600/mm grating. The microscope objective used for the studies was 100X. As excitation, it was used a 785 nm laser line with the power at the sample surface of 85 mW.

EPR measurements were carried out at room temperature using a Bruker ELEXSYS E500 spectrometer in X - band (9.4 GHz) and with a field modulation of 100 kHz. To avoid the alteration of the glass structure due to the ambient conditions, samples of equal quantities were enclosed immediately after preparation in quartz tubes of the same caliber.

Chapter 4

The results of $x\text{MnO} \cdot (100-x)[y\text{P}_2\text{O}_5 \cdot \text{CaO}]$

phosphate glasses study

4.1. Structural characteristics of $[y\text{P}_2\text{O}_5 \cdot \text{CaO}]$ binary glasses

4.1.1. Comparative study by X-Ray diffraction of $y\text{P}_2\text{O}_5 \cdot \text{CaO}$ glasses structure

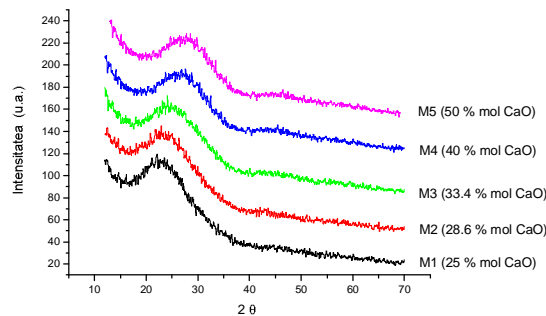


Fig. 4.1. X-Ray patterns for $y\text{P}_2\text{O}_5 \cdot \text{CaO}$ glasses

The XRD patterns obtained present a broad diffuse scattering at low angles which indicates a long-range structural disorder characteristic to vitreous solids. The first diffraction maximum is displacing to higher angles with increasing the CaO content in samples. From this displacing results that medium atomic distance is decreasing with increasing CaO content, therefore the phosphate network become much compactness.

4.1.2. Comparative study by IR absorption of $[yP_2O_5 \cdot CaO]$ glasses structure

In figure 4.3. and figure 4.4. are presented the experimental respectively, deconvolution of experimental IR spectra of the studied glasses. There are similarities between the spectra of the matrices due to the principles bands of the vitreous P_2O_5 that can be find in the investigated matrices shifted to the lower or higher wavenumber, and similarities due to the phosphate units that appear once with addition of the oxide modifiers CaO .

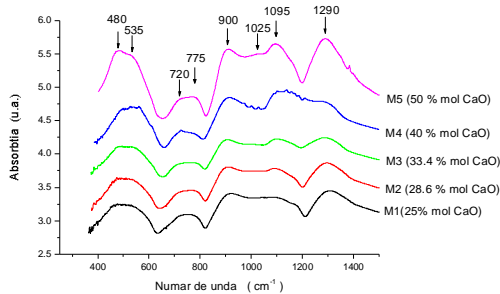


Fig. 4.3. IR absorption spectra of $yP_2O_5 \cdot CaO$ glasses

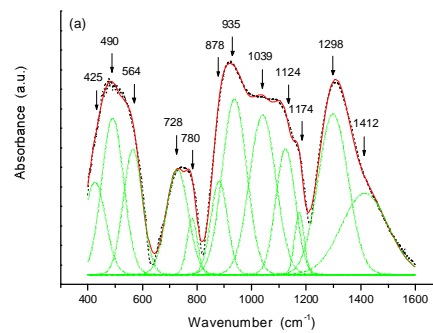


Fig. 4.4. Deconvoluted spectra of $yP_2O_5 \cdot CaO$ glasses

The results obtained for studied system by deconvolution procedure are:

The IR analysis reveals that the low wavenumber envelope around $400-566 \text{ cm}^{-1}$ consists of more than one absorption band. This envelope is resolved into three component bands at $\sim 400 \text{ cm}^{-1}$, $\sim 478 \text{ cm}^{-1}$ and $\sim 564 \text{ cm}^{-1}$. A shift towards lower wavenumbers of third component bands was observed on increasing CaO content. It was reported [2] that the band at about 400 cm^{-1} is attributed as the bending vibrations of $P-O$. The absorption band at 478 cm^{-1} is assigned to harmonics of bending vibrations of $O=P-O$ linkages [3] and the band at 560 cm^{-1} is attributed to bending vibrations of bridging phosphorus $\delta(O-P-O)$ on Q^1 structure [4]. We can observe (Table 2) that the amount of bridging phosphorous, as indicated by relative area, is increasing with CaO content. The change in the amount of these bridges may reflect the modification in the glass structure due to the depolymerization of the phosphate matrix with increasing CaO content from 25 to 50 mol %.

On the basis of previous observation [5] the band centred at 727 cm^{-1} can be assigned to a covalent bond between non-bridging oxygen and calcium ions as P-O-Ca stretching vibrations. The IR band at 776 cm^{-1} is assigned to symmetric stretching vibrations of P-O-P in rings [6-8] and this band increases slowly in intensity till $x = 33.4$ mol % and then, decreases due to the depolymerization of the phosphate network. Accordingly, with this, an increase of P-O-Ca stretching vibrations could be observed from 33.4 mol %.

The IR absorption in the region $850\text{-}1200\text{ cm}^{-1}$ was found to be sensitive for different metaphosphate groups in the form of chain-, ring- and terminal groups [10-11]. The spectral analysis of this region shows the existence of five bands: ~ 880 , ~ 930 , ~ 1020 , ~ 1120 and $\sim 1160\text{ cm}^{-1}$. The absorption band at $\sim 880\text{ cm}^{-1}$ is attributed to asymmetric stretching vibration of P-O-P groups linked with linear metaphosphate chain [9, 12], while that at 930 cm^{-1} is assigned to asymmetric stretching of P-O-P groups linked with large metaphosphate rings [11, 13]. The feature at $\sim 1020\text{ cm}^{-1}$ is attributed to asymmetric stretching of P-O-P groups, $\nu_{\text{as}}(\text{P-O-P})$ modes, linked with small metaphosphate rings as cyclotriphosphate [$\text{P}_3\text{O}_9^{3-}$] or smaller rings [11, 15]. The band at $\sim 1120\text{ cm}^{-1}$ is assigned to asymmetric stretching of PO_2^- group, $\nu_{\text{as}}(\text{PO}_2^-)$ modes [6, 8]. The 1174 cm^{-1} band is associated with the terminal phosphate groups, PO_3^{2-} [4].

The analysis of the IR spectra of the studied glasses reveals that the total content of P-O-P bridges with ring structures ($924\text{-}948\text{ cm}^{-1}$) decreases when increasing the CaO content. The decrease of the relative area of component bands produced by such ring structures is a good indication for the formation of terminal PO_3^{2-} and P-O-P groups with chain structure. The occurrence of a continuous breakdown of the ring type structures into short arrangements such as small metachains and terminal phosphate groups upon network depolymerization may also account for this behavior [17]. This development decreases the average length of phosphate chain structures.

The other two bands observed at about $\sim 1280\text{ cm}^{-1}$ and $\sim 1386\text{ cm}^{-1}$ have been attributed to the asymmetric stretching of the double bonded oxygen vibration [14] and to the (P=O) symmetric stretching vibration, respectively [16, 19]. The shift to lower wavenumber of P=O absorption band with increasing CaO content is possible due to the polarization effect of the modifying cation (Ca^{2+}). This suggestion is confirmed by the

appearance of the pyrophosphate band at 1091-1123 cm^{-1} . The change in the vibrational frequency of pyrophosphate groups with increasing CaO content causes a decrease in the P-O vibrations frequency from ~ 1123 to ~ 1091 cm^{-1} . The modification in the metaphosphate structure, resulting from increasing CaO content in glasses, can be interpreted in terms of the charge density change at the anionic site [11]. With increasing the CaO content, some of the ring structures (low condensed phosphate anions) open and form smaller structures such as short chains and terminal structures (high condensed phosphate anions). Thus, the charge density at the ring structure sites may decrease while that at chain structure and terminal sites may increase with increasing CaO content. The compactness in the glass matrix upon addition CaO is due to the increase of the cross-link density of calcium ions either by disrupting the bonds connecting neighboring PO_4 groups and/or by the conversion of metaphosphate rings into chain and terminal ones. In this respect, calcium ions provide ionic cross – linking between the non-bridging oxygens of different chains and/or groups. This cross-linking increases the bond strength of this ionic cross-link, consequently the glass strength is expected to be improved.

4.1.3. Comparative study by Raman effect of $[\text{yP}_2\text{O}_5\text{-CaO}]$ glasses structure

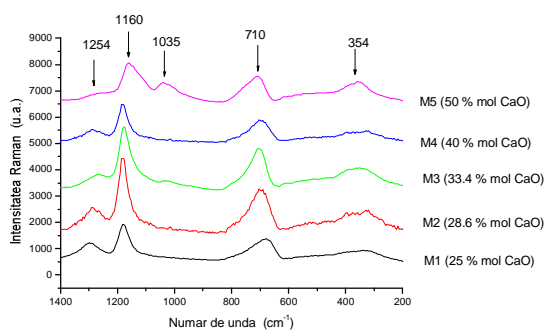


Fig. 4.6. Raman spectra of $\text{yP}_2\text{O}_5\text{-CaO}$ glasses

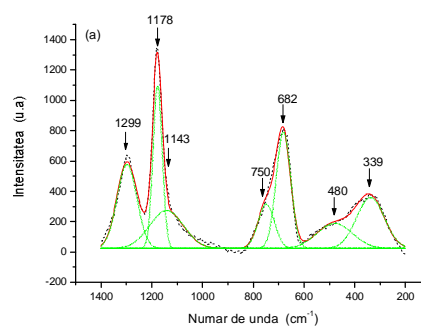


Fig. 4.7. Typical deconvoluted spectra of $\text{yP}_2\text{O}_5\text{-CaO}$ glasses

In figure 4.6. and figure 4.7. are presented the experimental respectively, deconvolution of experimental Raman spectra of the studied glasses. There are similarities between the spectra of the matrices due to the principles bands of the

vitreous P_2O_5 that can be found in the investigated matrices shifted to the lower or higher wavenumber.

The results obtained for the studied system by deconvolution procedure are:

Raman spectra for $25CaO \cdot 75P_2O_5$ ($x = 25$ mol %) glasses is given in Figure 4.7. The bands at 340 cm^{-1} and 480 cm^{-1} are attributed to the O-P-O bending and P-O-P bending, respectively [21]. The band at 682 cm^{-1} is attributed to the P-O-P symmetric stretching vibration [22]. Another band due to P-O-P symmetric stretching vibration is observed in metaphosphate spectrum at $\sim 750\text{ cm}^{-1}$ [23,24]. The band at 1143 cm^{-1} has been attributed to symmetric stretching motions of two non-bridging oxygen (NBO) atoms bonded to phosphorous atoms (PO_2) in the Q^2 phosphate tetrahedron [25]. The other two bands observed at 1178 cm^{-1} and 1299 cm^{-1} have been attributed to 'strained' (PO_2) symmetric (strained structural units, possibly three- or four-membered rings) [26] and to the P=O symmetric stretching [22, 26].

For higher content of calcium oxide ($x = 50$ %) when it clearly affects the phosphate network, a Raman spectrum is given in Figure 3(b). A new band appears at 1036 cm^{-1} with the increasing of the CaO content at $x \geq 33.33$ mol % and two features have been observed around 963 cm^{-1} and 1117 cm^{-1} for $x = 40$ mol %. The band at 1036 cm^{-1} is attributed to asymmetric stretching vibrations of $(PO_3)^{2-}$ of Q^1 species [27], whereas the band from 1117 cm^{-1} is due to (PO_3) symmetric stretching of the Q^1 [24]. The band at about 963 cm^{-1} is due to the (PO_4) symmetric stretching vibrations of the Q^0 species [24]. The band corresponding to 'strained' $(PO_2)_{sym}$ disappeared [18].

The intensities and the shifts of the Raman bands versus CaO content and the correlation of these data with the structural groups which appear in the studied glasses are also done.

The asymmetric 682 cm^{-1} band assigned to P-O-P symmetric stretching vibrations of the long-chain phosphate glasses is shifted to 702 cm^{-1} due to the decreasing of phosphate chain lengths [25, 29]. The shift of this band may be also attributed to a change in the in-chain P-O-P bond angle as an effect of the CaO network modifier on the glass structure [29]. The higher wavenumber of the P-O-P symmetric band is a result of the smaller P-O-P bond angle, characteristic for shorter phosphate chain length [21, 22]. A second P-O-P symmetric stretching vibrations band is observed in the metaphosphate spectrum at ca. 742 cm^{-1} [31]. This band may be due to very short chain phosphate units or ring structures [32], which are known to be increasingly

important in the composition region between the ultraphosphate (pure P_2O_5) and metaphosphate glasses. The higher wavenumber of this band relative to the band at ca. 695 cm^{-1} is consistent with shorter chains of phosphate units [33].

With the increase of CaO content, the bands characteristic to phosphate glasses (POP_{sym} stretch (Q^2), $(P=O)_{\text{sym}}$ stretch) decrease strongly in intensity, except the specific bands of the very short chain phosphate units or ring structure and $(PO_3)_{\text{asym}}$ stretch (Q^1). In the same time the band at 480 cm^{-1} which was attributed to the bending mode of the phosphate (PO_4) polyhedra increases strongly in intensity, too.

4.2. Structural characteristics of $xMnO \cdot (100-x)[yP_2O_5 \cdot CaO]$

ternary glasses

4.2.1. Comparative study by IR absorption

of $xMnO \cdot (100-x)[yP_2O_5 \cdot CaO]$ glasses structure

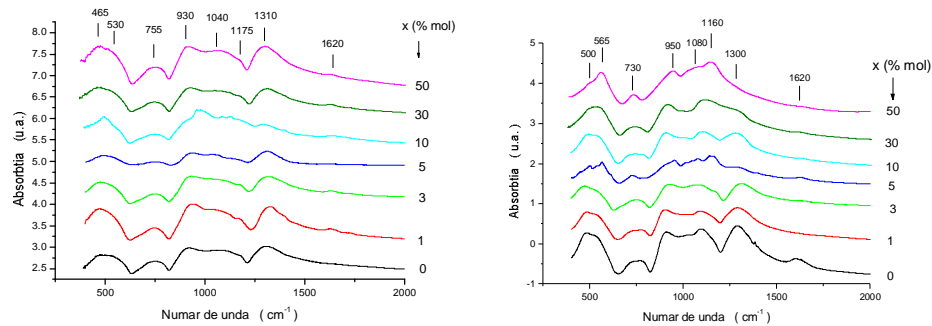


Fig.4.8a. and Fig.4.8e. IR absorption spectra of $xMnO \cdot (100-x)[yP_2O_5 \cdot CaO]$ glasses for S1 and S5 oxide systems

In figure 4.8a and 4.8e are presented IR absorption spectra for the systems S1 and S5 oxide systems. The spectra are typical for all 5 systems investigated. In all cases, it was done a deconvolution procedure and the results for the systems S5 it will be presented in the next table.

Table4.4e. IR band assignments and relative intensities for S5 glass system, x in mol % MnO

$\nu [\text{cm}^{-1}]$	Assignments	x=0	x=1	x=3	x=5	x=10	x=30	x=50
390-416	$\delta(P-O)$	6	3.1	5.6	4.5	5.1	8.5	7.8
470-500	$\delta(O=P-O)$	11	10.9	15.5	4.7	12.3	11.7	1.2
545-565	$\delta(O-P-O), Q^1$ species	10.6	14.1	7.3	9.5	5.4	9.1	14.8

685-715	$\nu(\text{P-O-Ca})$	4.4	5.3	9.8	2.5	2.1	1.4	2.5
763-781	$\nu(\text{P-O-P})$ in rings, Q^3 groups	1.6	2.1	2.1	1.8	2.4	3.2	1.5
875-897	$\nu_{\text{asym}}(\text{P-O-P})$, linear metaphosphate chain, Q^2	4.6	5.7	6.8	11.8	8.9	15	24.2
924-966	$\nu_{\text{asym}}(\text{P-O-P})$, large metaphosphate rings	9.7	8.6	8.4	1.2			
1001-1071	$\nu_{\text{asym}}(\text{P-O-P})$, small metaphosphate rings	10.5	11.5	11.4	8.5	15.7	9.7	11.2
1091-1133	$\nu_{\text{as}}(\text{PO}_2^-)$ modes	11.9	9.7	7.2	2.5	7.2	13	15.5
1157-1183	terminal phosphate groups, PO_3^{2-}	1.6	1.7	1.6	11.2	7.8	13	5.1
1279-1312	$\nu_{\text{asym}}(\text{P=O})$	15.7	18.8	12.2	12.2	9	11	11.4
1402-1454	$\nu_{\text{sym}}(\text{P=O})$	12.4	8.6	12.2	1.2	4.4	4.4	4.8

The results obtained after the deconvolution procedure in all cases are:

- Characteristic metaphosphate bands are decreasing in intensity with increasing MnO content, exception is in the case of the band assignment to the linear metaphosphate chain for S3 ÷ S5 glass system which is increasing in all concentration range.
- The band specific to Q^1 groups is increasing with increasing manganese ions number.
- The band centred at $\sim 1174 \text{ cm}^{-1}$ associated with terminal phosphate groups PO_3^{2-} is increasing in intensity from where results that the number of nonbonding oxygen are increasing.
- In all systems studied the presence of the water results from the bands apparition at $\sim 1620 \text{ cm}^{-1}$, which is assigned to bending vibration of H-O-H [23, 24].
- For grater concentration of MnO in all investigated systems it can be seen an increasing of the local order.

4.2.2. Comparative study by Raman effect of $x\text{MnO} \cdot (100-x)[y\text{P}_2\text{O}_5 \cdot \text{CaO}]$ glasses structure

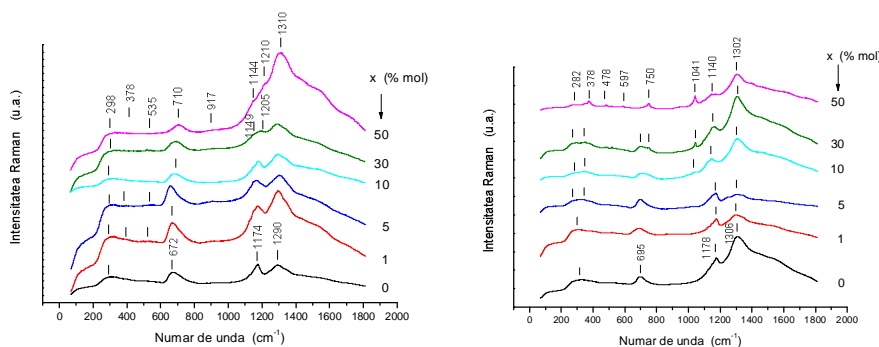


Fig.4.10. Raman spectra of $x\text{MnO} \cdot (100-x)[y\text{P}_2\text{O}_5 \cdot \text{CaO}]$ glasses for S1 and S5 oxide systems

In figure 4.10a and 4.10e are presented Raman spectra for the systems S1 and S5 oxide systems. Wavenumbers and their assignments for Raman spectra of S1÷S5 glass systems are presented in Table 4.6. The principales results obtained in all investigated systems are:

Table 4.6. Wavenumbers and their assignments for Raman spectra of S1÷S5 glass systems

Wavenumber (cm^{-1})					Assignments
S1	S2	S3	S4	S5	
298	272	301	300	282	bending vibrations of the phosphate polyhedra
378	380	380	380	378	O-P-O bending modes
535	540	550	550	597	symmetric stretching of P-O- bonds
710	710	692	700	750	symmetric stretching mode of P-O-P bridging oxygens, $(\text{POP})_{\text{sym}}$, between Q^3 phosphate tetrahedra
917	910	897	900	900	symmetric stretching vibrations of isolated $(\text{PO}_4)^{3-}$, associated with Q^0 tetrahedra
			1040	1041	asymmetric stretching vibrations of $(\text{PO}_3)^{2-}$, Q^1 species
1144	1145	1178	1150	1140	symmetric stretching mode of O-P-O non-bridging oxygens, $(\text{PO}_2)_{\text{sym}}$, Q^2 phosphate tetrahedra
1210	1216				symmetric stretching mode of O-P-O, Q^2 phosphate tetrahedra
1310	1297	1309	1308	1302	symmetric stretching of the P=O terminal oxygens, $(\text{P=O})_{\text{sym}}$, associated with Q^3 tetrahedra

- The structural units presents in all investigated systems are similar and characteristic to methaphosphate structure, until 5 mol % MnO [36].
- Liniar methaphosphate chain are breaking with increasing of MnO content [37].
- The phosphate network is changing gradual from methaphosphate structure in one where are presented ortho- and phyrophosphate units, with increasing of manganese content.
- The vitreous matrix are different changed by manganese ions: S3 system isn't change very much with additions of MnO; in the case of S1, S2, S4, S5 systems, it can be observed a relative increase of local order in phosphate network, for higher concentrations of MnO.

4.2.3.Comparative study by EPR of $x\text{MnO}\cdot(100-x)[y\text{P}_2\text{O}_5\cdot\text{CaO}]$ glasses structure

Recorded EPR spectra show the resonance lines due to Mn^{2+} paramagnetic ions for all investigated concentrations. The shape of the EPR spectra strongly depends on the MnO content of the samples and on the matrice compositions. In figure 4.11a and 4.11e are presented EPR spectra for the systems S1 and S5 oxide systems.

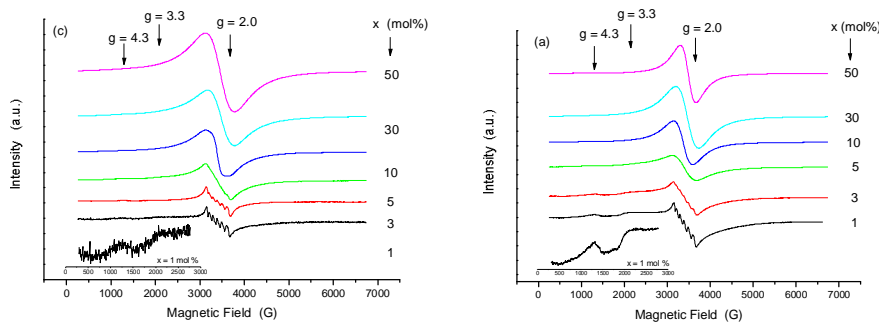


Fig.4.11. EPR spectra of $x\text{MnO}\cdot(100-x)[y\text{P}_2\text{O}_5\cdot\text{CaO}]$ glasses for S1 and S5 oxide systems

The spectra consist mainly of resonance lines centered at g -factor values of $g_{\text{eff}} \cong 2.0$, $g_{\text{eff}} \cong 4.3$ and $g_{\text{eff}} \cong 3.3$, their relative intensity depending on the manganese content of the samples as shown in figure 4.11. This isotropic signal at $g_{\text{eff}} \cong 2.0$ is due to isolated Mn^{2+} ions in an environment close to octahedral symmetry. The g - factor value and the well

resolved hyperfine structure (hfs) with a coupling constant of $A \cong 100$ G show the predominantly ionic character of the bonding between Mn^{2+} and O^{2-} ions generating the octahedral symmetry of the ligand field. Weak axial distortions could be superimposed on this field, varying in intensity and orientation from the vicinity of manganese ions to another [44, 45]. The hfs superimposes on a large absorption line, which could be due to the dipol-dipol or superexchange magnetic interaction. The strongly distorted versions of the octahedral vicinity, subjected to strong crystal field effects, give rise to absorptions at $g_{eff} \cong 4.3$ and $g_{eff} \cong 3.3$ (Fig. 1). These absorptions are less intense than the one at $g_{eff} \cong 2.0$ and appear only for low concentrations of manganese ($x \leq 5$ mol %). There is a relatively small concentration of Mn^{2+} ions involved in such structural units. The lack of hfs at these absorption lines is due to the fluctuations of the ligand field parameters in the Mn^{2+} ion neighborhood and the random distribution of the octahedral distortions vicinity [46].

The evolution of the resonance lines with the increase of manganese ions content can be followed in the dependence of the EPR characteristic parameters, i.e. the peak-to-peak linewidth, ΔB and the line intensity, J . The corresponding variations of these parameters are plotted in figure 4.15 for the resonance line centered at $g_{eff} \cong 2.0$. As one can see, ΔB and J show different evolutions for these five series of investigated samples.

For all investigated systems, the linewidth increases linear with the MnO content up to $x = 5$ mol % due to the increase of the dipolar interaction between the Mn^{2+} ions [17, 18]. In the case of S1÷S4 systems, for $5 \text{ mol \%} \leq x \leq 10 \text{ mol \%}$, the linewidth increases, but much slowly and in this range could appear superexchange interactions.

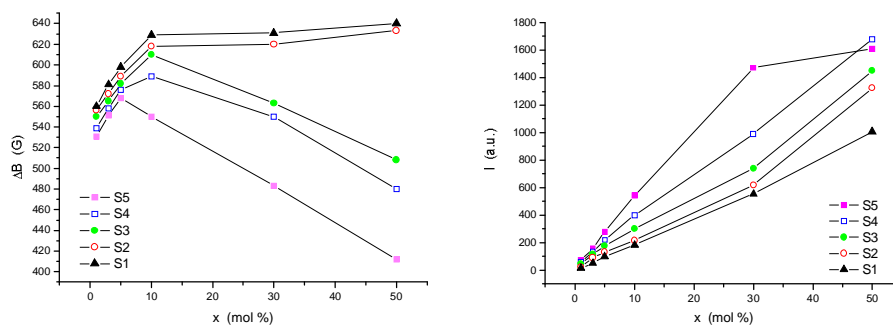


Fig. 4.15 Composition dependence of the peak-to-peak linewidth, ΔB and the line intensity, J for S1÷S5 systems.

Above 10 mol %, for S1 and S2, the linewidth continue to increase but very slowly and in this range coexist the dipol-dipol and superexchange magnetic interaction and their intensity are \sim equal. For higher concentrations, $x \geq 10$ mol % and $x \geq 5$ mol %, respectively in the case of S3, S4 and S5 it could be observed a strong decrease of the linewidth which could be attributed to a superexchange – type interaction between the manganese ions close enough to each other. Such doping levels of the samples impose the progressive clustering of manganese ions.

Generally, the signal intensity is proportional to the number of EPR active species involved in the resonance absorption. For all investigated sample, the intensity, J of the resonance line at $g_{\text{eff}} \cong 2.0$ increases with the increase of x in the whole concentration range. Above 30mol %, the corresponding increase is very slowly. The non-linear increase of J with manganese concentration shows that manganese ions in $x\text{MnO} \cdot (100-x)[y\text{P}_2\text{O}_5 \cdot \text{CaO}]$ glasses are present as Mn^{2+} as well as Mn^{3+} [49, 59].

In figure 4.17 are presented the temperature dependence of integral intensity for systems S1 and S5. It could be observed that these dependence are linear typical for Curie-Weiss law. From these dependence one could evaluate the paramagnetic Curie temperature θ_p . The evaluated temperatures are presented in Table 4.8.

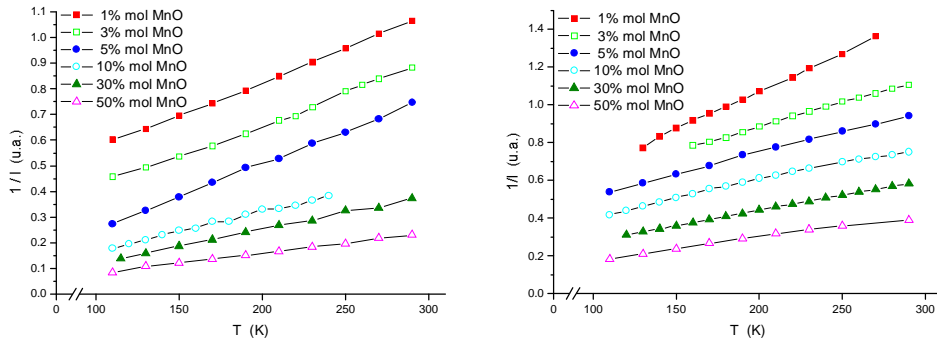


Fig. 4.17 Temperature dependences of $1/I$ for systems S1 and S5.

All evaluated θ_p are negative values. In the low range of MnO concentrations these values are closed to 0 K, from where results that in this composition range manganese ions presents are isolated and presents a paramagnetic behavior. For higher concentration of MnO, antiferromagnetic behavior is increasing, this behavior could be observed with increasing of CaO content, also.

Table 4.8. Paramagnetic Curie temperature, θ_p .

Sistems	θ_p (K)					
	1% mol MnO	3% mol MnO	5% mol MnO	10% mol MnO	30% mol MnO	50% mol MnO
S1	- 2K	- 4K	- 10K	- 14K	- 34K	- 60K
S3	- 3K	- 4K	- 12K	- 26K	- 38K	- 80K
S5	- 3K	- 7K	- 16K	- 53K	- 74K	- 155K

SELECTED REFERENCES

- [1.20] R. K. Brow, *J. Non-Cryst Solids*, 263&264, 1 (2000)
- [4.1.2] C. Dayanand, G. Bhikshamaiah, V. Jaya Tyagaraju, M. Salagram, A.S.R. Krishna Murty, *J. Mat. Sci.* 31, 1945 (1996)
- [4.1.3] K. El-Egili, H. Doweidar, Y.M. Moustafa, I. Abbas, *Physica B*, 339, 237 (2003)
- [4.1.4] M. Efimov, *J. Non-Cryst. Solids* 209, 209 (1997)
- [4.1.5] S.M. Abo-Naf, M.S. El-Amiry, A. A. Abdel-Khalek, *Optical Materials* 30, 900 (2008)
- [4.1.6] M.C.R. Shastry, K. Rao, *J. Spectrochim. Acta A*, 46, 209 (1990)
- [4.1.7] J.P. Malugani, R. Mercier, *Solid State Ionics* 13, 293 (1984)
- [4.1.8] M. Scagliotti, M. Villa, G. Chiodelli, *J. Non-Cryst. Solids* 93, 350 (1987)
- [4.1.9] W.P.G. Griffith, *J. Chem. Soc. A*, 905 (1967)
- [4.1.10] E.I. Kamitsos, A.P. Patsis, M.A. Karakassides, G.D. Chryssikos, *J. Non-Cryst. Solids* 126, 52 (1990)
- [4.1.11] E.I. Kamitsos, J.A. Kapoutsis, G.D. Chryssikos, J.M. Hutchinson, A.J. Pappin, M.D. Ingram, J.A. Duffy, *Phys. Chem. Glasses* 36 (3), 141 (1995)
- [4.1.12] A. Rulmont, R. Cahay, M. Liegeois-Duychaerts, P. Tarte, *Eur. J. Solid state Inorg. Chem.* 28, 207 (1991)
- [4.1.13] D.E.C. Corbridge, E.J. Lowe, *J. Chem. Soc.* 57, 4555 (1954)
- [4.1.14] B.V.R. Chowdari, K.I. Tan, W.T. Chia, R. Gopalakrishnam, *J. Non-Cryst. Solids*, 119, 95 (1990)
- [4.1.15] Y.M. Moustafa, K. El-Egili, *J. Non-Cryst. Solids* 240, 144 (1998)
- [4.1.16] J.J. Hudgens, S.W. Martin, *J. Am. Ceram. Soc.* 76, 1691 (1994)
- [4.1.17] **D. Toloman**, D.A. Magdas, I. Bratu, L.M. Giurgiu, I. Ardelean, *Int. J. Modern Phys. B* – acceptata pentru publicare
- [4.1.18] **D. Toloman**, A.R. Biris, D. Maniu, I. Bratu, L.M. Giurgiu, I. Ardelean, *J. Partic. Sci. Technol.* - acceptata pentru publicare
- [4.1.19] D.A. Magdas, O. Cozar, I. Ardelean, L. David, *J. Optoelectron. Adv. Mater.* 9, 729 (2007)
- [4.1.21] J. Koo, B. Bae and H.K. Na, *J. Non-Cryst. Solids*, 212, 173 (1997)
- [4.1.22] M. Scagliotti, M. Villa and G. Chiodelli, *J. Non-Cryst. Solids*, 93, 350 (1987)
- [4.1.23] O. Cozar, D. A. Magdas, L. Nasdala, I. Ardelean and G. Damian, *J. Non-Cryst. Solids* 352, 3121 (2006)
- [4.1.24] M.A. Karakassides, A. Saranti, I. Koutselas, *J. Non-Cryst. Solids*, 347, 69 (2004)

- [4.1.25] J.E. Pemberton, L. Latifzadeh, J.P. Fletcher and S.H. Risbud, *Chem. Mater.*, 3, 1995 (1991)
- [4.1.26] J.J. Hudgens, R.K. Brow, D.R. Tallant and S.W. Martin, *J. Non-Cryst. Solids*, 223, 21 (1998)
- [4.1.27] S.T. Reis, D.L.A. Faria, J.L. Martinelli, W.M. Pontuschka, D.E. Day and C.S.M. Partiti, *J. Non-Cryst. Solids*, 304, 188 (2002)
- [4.1.29] A. Bertoluzza, M.A. Battaglia, R. Simoni and D.A. Long, *J. Raman Spectrosc.*, 14, 178 (1983)
- [4.1.32] B.N. Nelson and G.J. Exarhos, *J. Chem. Phys.*, 71 2739 (1979)
- [4.1.3] H.J. Becher, *J. Less-Common Met.*, 76, 169 (1980)
- [4.2.17] **D. Toloman**, C. Tripon, L.M. Giurgiu, I. Ardelean, *J. Optoelectron. Adv. Mat.* 8 (3), 1109 (2006)
- [4.2.18] **D. Toloman**, C. Tripon, I. Bratu, O. Raita, L.M. Giurgiu, I. Ardelean, *Studia Universitatis Babes-Bolyai, Physica, L*, 4a, 487 (2005)
- [4.2.23] C. Tripon, **D. Toloman**, O. Cozar, I. Bratu and I. Ardelean, *Studia Universitatis Babes-Bolyai, Physica, L*, 4b, 624 (2005)
- [4.2.24] C. Tripon, **D. Toloman**, M. Aluas, C. Filip and I. Ardelean, *J. Optoelectron. Adv. Mat.*, 8, No. 3, 1129 (2006)
- [4.2.36] **D. Toloman**, A.R. Biris, A. Popa, O. Raita, L.M. Giurgiu, I. Ardelean, *J. Physics: Conference Series* 182, 012032 (2009)
- [4.2.37] **D. Toloman**, A.R. Biris, A.S. Biris, I. Ardelean, *J. Partic. Sci. Technol.* – acceptata pentru publicare
- [4.2.44] M. Peteanu, I. Ardelean, S. Filip, D. Alexandru, *Rom. J. Phys.* 41, 593 (1996)
- [4.2.45] I. Ardelean, S. Filip, *J. Optoelectron. Adv. Mater.* 5(1), 157 (2003)
- [4.2.46] V. Cerny, B. Frumarova, J. Borsa, I.L. Licholit, M. Frumar, *J. Non-Cryst. Solids* 192-193, 165 (1995)
- [4.2.49] R.K. Singh, A. Srinivasan, *J. Magn. Mater.* 321, 2749 (2009)
- [4.2.59] **D. Toloman**, L.M. Giurgiu, I. Ardelean, *Physica B*, 404, 4198 (2009)

SELECTED CONCLUSIONS

In this thesis, $x\text{MnO}\cdot(100-x)[y\text{P}_2\text{O}_5\cdot\text{CaO}]$ glass system, with $y = 1\div 3$ and $0 \leq x \leq 50$ mol % MnO were comparatively studied. The structural modifications of investigated glass matrices were comparatively followed in function of vitreous network modifiers and also regarding the influence of the manganese ions on the investigated glass matrices.

The study by X-ray diffraction of vitreous matrices $y\text{P}_2\text{O}_5\cdot\text{CaO}$ evidenced the followings:

- The XRD patterns obtained present a broad diffuse scattering at low angles which indicates a long-range structural disorder characteristic to vitreous solids.
- The first diffraction maxim is displacing to higher angles with increasing the CaO content in samples. From this displacing results that medium atomic distance is decreasing with increasing CaO content, therefore the phosphate network become much compactness.

The study by IR absorption spectroscopy of vitreous matrices $y\text{P}_2\text{O}_5\cdot\text{CaO}$ evidenced the followings:

- IR spectral analysis shows that increasing CaO content leads to a breakdown of the ring type structures.
- Calcium ions provide ionic cross – linking between the non-bridging oxygen of different chains and/or groups, this cross-linking increases the bond strength. Consequently the glass strength is expected to be improved

The study by Raman spectroscopy of vitreous matrices $y\text{P}_2\text{O}_5\cdot\text{CaO}$ evidenced the followings:

- The phosphate glass characteristic bands strongly decrease in intensity except the specific bands of the very short chain phosphate units or ring structures and to the (PO_4) symmetric stretching vibrations of the (Q^0) group which become more intense with the increasing of CaO content.
- The 682 cm^{-1} band assigned to the P-O-P symmetric stretching vibrations is also shifted up to 702 cm^{-1} due to the decrease of the chain length.

- For higher content of calcium oxide ($x = 40 \%$), new bands appear at about 963 cm^{-1} and 1117 cm^{-1} characteristic to (PO_4) symmetric stretching vibrations of the Q^0 species and to (PO_3) symmetric stretching of the Q^1 , respectively.

The study by IR absorption spectroscopy of $x\text{MnO} \cdot (100-x)[y\text{P}_2\text{O}_5 \cdot \text{CaO}]$ glass systems evidenced the followings:

- Characteristic methaphosphate bands are decreasing in intensity with increasing MnO content, exception is in the case of the band assignment to the linear methaphosphate chain for S3 ÷ S5 glass system which is increasing in all concentration range.
- The band specific to Q^1 groups is increasing with increasing manganese ions number.
- The band centred at $\sim 1174 \text{ cm}^{-1}$ associated with terminal phosphate groups PO_3^{2-} is increasing in intensity from where results that the number of nonbonding oxygen are increasing.
- For grater concentration of MnO in all investigated systems it can be seen an increasing of the local order.

The study by Raman spectroscopy of $x\text{MnO} \cdot (100-x)[y\text{P}_2\text{O}_5 \cdot \text{CaO}]$ glass systems evidenced the followings:

- The structural units presents in all investigated systems are similar and characteristic to methaphosphate structure, until 5 mol % MnO.
- Linear methaphosphate chain are breaking with increasing of MnO content.
- The phosphate network is changing gradual from methaphosphate structure in one where are presented ortho- and phyrophosphate units, with increasing of manganese content.
- The vitreous matrix are different changed by manganese ions: S3 system isn't change very much with additions of MnO; in the case of S1, S2, S4, S5 systems, it can be observed a relative increase of local order in phosphate network, for higher concentrations of MnO.

The study by EPR of $x\text{MnO} \cdot (100-x)[y\text{P}_2\text{O}_5 \cdot \text{CaO}]$ glass systems evidenced the followings:

- The distribution of Mn^{2+} ions in several structural units of the glasses was revealed by the EPR spectra, the structure depending of the MnO content. In the low concentration range ($x \leq 5 \text{ mol } \%$), the Mn^{2+} ions were identified in sites of

octahedral symmetry giving rise to an absorption line centered at $g_{\text{eff}} \cong 2.0$. Strongly distorted versions of these sites result in the resonance lines at $g_{\text{eff}} \cong 4.3$ and $g_{\text{eff}} \cong 3.3$. The intensity of last two lines is small enough and indicates a relative low concentration of Mn^{2+} ions involved in such structural units.

- The g - factor value and the well resolved hyperfine structure (hfs) with a coupling constant of $A \cong 100$ G show the predominantly ionic character of the bonding between Mn^{2+} and O^{2-} ions.
- The linewidth dependence on MnO content for the resonance line centered at $g_{\text{eff}} \cong 2.0$ indicates a structural modification in Mn^{2+} vicinity and the increase of dipolar interaction which is accompanied by the superexchange magnetic interaction.
- From the non-linear increase of line intensity with manganese concentration results that the manganese ions are presented as Mn^{2+} as well as Mn^{3+} in the investigated samples.
- From the values of θ_p closed to 0 K results that manganese ions presents are isolated and presents a paramagnetic behavior in the low range of MnO concentrations. For higher concentration of MnO, antiferromagnetic behavior is increasing, this behavior could be observed with increasing of CaO content, also.
- The vitreous structure of our glasses show an evolution with the MnO content from the structural units involving Mn^{2+} ions in well-defined vicinities having certain symmetry to structural units containing clustered magnetic ions.